Experimental and simulated distribution and interaction of water in cellulose esters with alkyl chain substitutions

Carbohydrate Polymers 306 (2023) 120616

Contents lists available at ScienceDirect

Carbohydrate Polymers

journal homepage: www.elsevier.com/locate/carbpol

Experimental and simulated distribution and interaction of water in cellulose esters with alkyl chain substitutions

Robin Nilsson [a,b], Hüsamettin Deniz Özeren [c], Okky Dwichandra Putra [d], Mikael Hedenqvist [c,e,f], Anette Larsson [a,b,g,*]

[a] Applied Chemistry, Department of Chemistry and Chemical Engineering, Chalmers University of Technology, SE-412 96 Gothenburg, Sweden
[b] FibRe Centre for Lignocellulose-based Thermoplastics, Department of Chemistry and Chemical Engineering, Chalmers University of Technology, SE-412 96 Gothenburg, Sweden
[c] Division of Glycoscience, Department of Chemistry, AlbaNova University Centre, KTH Royal Institute of Technology, SE-106 91 Stockholm, Sweden
[d] Early Product Development and Manufacturing, Pharmaceutical Sciences, R&D, AstraZeneca Gothenburg, Pepparedsleden 1, Mölndal SE-431 83, Sweden
[e] Wallenberg Wood Science Center, KTH Royal Institute of Technology, Stockholm, Sweden
[f] FibRe Vinnova competence center, KTH Royal Institute of Technology, Stockholm, Sweden
[g] Wallenberg Wood Science Center, Chalmers University of Technology, Gothenburg, Sweden

ARTICLE INFO

Keywords:
Water interactions
Hysteresis
Simulations
Cellulose acetate

ABSTRACT

This study investigated the effect of the average length of substituted side chains in different cellulose esters on water sorption and the water association mechanism. For this purpose, a set of esters with a similar total degree of substitution was selected: cellulose acetate, cellulose acetate propionate, and cellulose acetate butyrate. Dynamic vapor sorption was used to determine the effect of the side chain length on sorption, desorption, and the occurrence of water clustering. Since water association in the structure was of interest, molecular dynamics simulations were performed on cellulose acetate and cellulose acetate propionate. This study showed that cellulose acetate appears to be water-sensitive and experiences hysteresis upon water sorption, which was attributed to structural changes. The simulations also showed that water is screened out by the side chains and forms intermolecular hydrogen bonds, primarily to the carbonyl oxygen rather than the residual hydroxyl groups.

1. Introduction

Cellulose derivatives have been researched for a long time due to their potential to replace fossil-based plastics in areas such as packaging. A few of the benefits of cellulose are its abundance, its ability to be obtained from various sources, such as plants and wood, its ability to be modified into derivatives with specific properties, and its resulting suitability for many applications, like pharmaceutics, barrier materials, laminates, coatings, and foods (Klemm et al., 2005). One common way to modify cellulose is via esterification of the anhydroglucose units in the cellulose molecules forming, for example, cellulose acetate (CA), cellulose acetate propionate (CAP), and cellulose acetate butyrate (CAB). These cellulose esters are commonly used polymers in barrier materials, coatings, sealants, foods, pharmaceutics, and osmosis applications (Gabor & Titia, 2012; Klemm et al., 2005; Schuetzenberger & Dreyfus, 2016). Not only can cellulose derivatives be produced from renewable resources, but their properties can be tailored to suit various application areas.

It is well-known that carbohydrates, like cellulose and other biopolymers, are sensitive to water. Water can absorb into and interact with biopolymers to induce plasticization, which has been observed for different bio-based polymers (Nilsson et al., 2022; Reid & Levine, 1991; Roos, 1995). Relative humidity (RH) and temperature are two environmental factors that affect the amount of water absorbed and, therefore, the net amount of plasticization obtained. The water-induced plasticizing of bio-based polymers may decrease desirable functionalities like barrier properties and mechanical strength. In the pursuit of better tailoring of humidity-resistant materials, it is crucial to predict the relationship between the amount of water absorbed and its effect on the properties of the materials. CA has been frequently studied for water

* Corresponding author at: Applied Chemistry, Department of Chemistry and Chemical Engineering, Chalmers University of Technology, SE-412 96 Gothenburg, Sweden.
E-mail addresses: robnils@chalmers.se (R. Nilsson), ozeren@kth.se (H.D. Özeren), okky.putra@astrazeneca.com (O.D. Putra), mikaelhe@kth.se (M. Hedenqvist), anette.larsson@chalmers.se (A. Larsson).

https://doi.org/10.1016/j.carbpol.2023.120616
Received 28 June 2022; Received in revised form 12 December 2022; Accepted 20 January 2023
Available online 24 January 2023

sorption and diffusion in membrane applications in the separation of, for example, salts and the effect of the degree of substitution (DS) of different side chains (Lonsdale et al., 1965; Ong et al., 2012, 2013; Palin et al., 1975; Qiao et al., 2012; Sun et al., 2013).

Asai et al. showed, via thermal investigations, that there are two mechanisms for water absorption in CA. One mechanism is controlled by the number of hydroxyl groups, where a decrease in hydroxyl groups and the corresponding increase in acetyl groups, results in less water absorbed. The other mechanism is controlled by the free volume, which is affected by the DS of acetyl groups, where an increase in DS increases the free volume (Asai et al., 2001; Ong et al., 2013). Asai et al. and Ong et al. also showed that the glass transition temperature (T_g) decreased with an increased DS of acetyl groups due to a decrease in hydrogen bonds from hydroxyl groups (Asai et al., 2001). The thermal properties are closely related to the mechanical properties, which have been shown to decrease with an increase in humidity (Gårdebjer et al., 2014). For cellulose, it is known that water can be present in three forms, namely, freezing, non-freezing, and bound freezing water (Hatakeyama & Hatakeyama, 1998). These forms can be explained as normal bulk water, water closely associated with the polymer, and water less associated with the polymer, respectively. A study on CA by Keely et al. concluded that it could be plasticized by both closely associated and less associated water (Keely, 2003). This could mean that even small amounts of water can alter the properties of CA.

Nilsson et al. investigated a set of cellulose esters and found that an increase in the average length of the ester moiety from CA to CAB increased the amount of dispersion energy in the material. This increased length of hydrophobic side-groups screened the possibilities for water to interact and form hydrogen bonding sites. Since the high T_g of CA partly originates from intermolecular hydrogen bonding, the screening via the addition of longer side chains, i.e., increasing the side chain by two methylene groups from acetyl to butyryl, decreased the T_g from 193 to 109 °C (Nilsson et al., 2022). This study was limited to dry and fully wet materials, where the first was dried in an oven at 60 °C and the second was submerged in room-tempered distilled water for 24 h. To further elucidate how water interacts with the materials, varying water contents through varying RH is required.

A common phenomenon for water-sensitive materials is hysteresis, which occurs due to a difference in the absorption and desorption of water. Many biopolymers, including starch (Rajabnezhad et al., 2020), chitosan, and microcrystalline cellulose (Agrawal et al., 2004; Driemeier et al., 2012), exhibit hysteresis. CA has been reported to show hysteresis and a sorption isotherm of type II (del Gaudio et al., 2021) when non-fibrous CA was used. In contrast, Simon et al. showed less significant hysteresis, possibly due to the use of CA fibers (Simon et al., 2021). Using dynamic vapor sorption (DVS), del Gaudio et al. demonstrated that the addition of two plasticizers to CA (diethyl phthalate and triphenyl phosphate) decreased the water absorption and the hysteresis. This decrease was attributed to the interaction of the plasticizer via hydrogen bonding, which decreased the available active sites for polymer-water hydrogen bonding.

Sorption and desorption isotherms from DVS measurements have been compared to several models, a popular one being the Guggenheim–Anderson–Boer (GAB) theory, as described by van den Berg (van den Berg, 1984van), which has been used in multiple studies on materials like flour, proteins, tea, wood, corn starch, polyethylene terephthalate, and CA (Alamri et al., 2018; Alipour et al., 2019; Arslan & Toğrul, 2006; Bratasz et al., 2012; Lopez-Silva et al., 2021; Vopička & Friess, 2014). The GAB model predicts the mass uptake of water (M) according to Eq. (1):

$$M = m_0 \frac{C_G K a_W}{(1 - K a_w)(1 + (C_G - 1) K a_W)} \quad (1)$$

where m_0 is the water molecules in a monolayer and indicates the active sites on the polymer that are available for water. C_G is the Guggenheimer constant and represents the strength of water-binding, primarily to the polymer. The constants K and C_G are parameters that, according to the model, should fulfill $0 < K \leq 1$ and $C_G > 0$. The values of C_G indicate different Brunauer's classifications of isotherms, where $C_G \geq 2$ means type II and $0 < C_G < 2$ means type III (Blahovec & Yanniotis, 2008, 2010; Brunauer et al., 1940).

The GAB model can thus provide information about how materials behave at different RH and the number of available interaction sites for water on the polymers. It does not provide any information about the identity of the interaction sites. To determine exactly which sites water interacts with, more investigations are needed. A promising method is molecular dynamics (MD) simulations, which has been used to model atomic and molecular motions, indicating how molecular orientation, velocities, and positions change over time. So far, MD has been used in numerous studies; in pharmacy it has been used to simulate polymer-drug interactions in aqueous solutions for oral drug delivery, swelling of cellulose crystals, hydrogen bonding in crystalline cellulose, and plasticization in starch (Bergenstråhle et al., 2010; Mosquera-Giraldo et al., 2018; Özeren et al., 2020a,b, 2021). For CA, MD has been performed for moisture diffusion and has shown good agreement between experimental and simulated data, making it a promising tool for CA-water systems. To the authors' knowledge, no study has thus far investigated the effect of ester average side chain length on water vapor sorption and water distribution with the help of MD simulations.

This study aims to investigate how water is distributed and interacts with the cellulose derivatives, CA, CAP, and CAB. The CAP and CAB used in this study are mixed esters, meaning they have a mix of propionyl and acetyl groups, and butyryl and acetyl, respectively, see Table 1. It is hypothesized that the carbonyl oxygens of the esters are the preferred water integration sites rather than the other oxygens in the cellulose esters. The increase in the average length of the side chain, from acetyl to propionyl (mixed ester CAP) to butyryl (mixed ester CAB), should screen the carbonyl oxygen, resulting in fewer available hydrogen bonding sites, therefore, less water sorption. We also hypothesize that CA has a higher probability of forming water clusters compared to esters with longer side chains. To investigate these hypotheses, a set of esters were studied, namely, CA, mixed ester CAP, and three mixed esters of CAB. All the studied esters had a high total DS (2.41–2.85, Table 1) but with different ratios of acetyl-propionyl and acetyl-butyryl groups. The distribution patterns of the mixed esters have not been investigated but could have an impact on the results. One cellulose ether, ethyl cellulose (EC), was also investigated as an outlier, with a similar total DS to the esters. MD simulations were used to study intermolecular distances between water and the different hydrogen bonding sites in the cellulose derivatives. Additionally, the MD simulations were used to investigate intermolecular changes by comparing distances between the different oxygens in the ester at low and high RH. The probability of clustering of water molecules was also experimentally investigated with GAB and MD simulations for both CA and CAP.

2. Experimental

2.1. Materials

Five different esters were bought from Sigma-Aldrich (Saint Louis, USA), including CA, CAP, and CAB with three DS of butyryl (CABI, CABII, and CABIII), Table 1. EC, ETHOCEL standard 14 premium was purchased from DOW (Bomlitz, Germany). The same starting material was used for structural characterization in this work as in Nilsson et al., see Table 1. The DS is stated as total DS (DS_{tot}), DS of acetyl (DS_A), DS of propionyl (DS_P), or DS of butyryl (DS_B), together with the degree of hydroxyl groups (D_{OH}). Other results are also summarized, including T_g, water absorption for fully submerged samples, and the amount of water per repeating unit at that absorption (Nilsson et al., 2022). The esters were mixed esters thus the term “average side chain length” is used when discussing the change in ratios between acetyl-propionyl or acetyl-

Table 1
DS, calculated from NMR, where DS_{tot} is the total DS, which, together with D_{OH} (degree of hydroxyl groups), adds up to three. DS_A, DS_P, and DS_B denote DS of acetyl, propionyl, and butyryl, respectively. DS values, T_g, and water absorption are from Nilsson et al. (Nilsson et al., 2022).

Material	DS_{tot}	DS_A	DS_P/DS_B	D_{OH}	Mn[a]	T_g [°C]	Water abs [wt%]	Water molecules per repeating unit
CA	2.41	2.41	–	0.59	50	193	12.0 ± 2.0	1.75
CAP	2.85	0.21	2.64	0.15	75	143	3.8 ± 0.2	0.67
CABI	2.85	2.14	0.71	0.15	65	154	4.4 ± 0.2	0.74
CABII	2.80	1.12	1.68	0.20	30	136	3.3 ± 0.1	0.61
CABIII	2.71	0.14	2.57	0.29	30	109	1.8 ± 0.5	0.35
EC	2.55	–	–	0.45	n.d.[b]	126	4.9 ± 0.2	0.64

[a] The molecular weights (Mn) are according to the supplier.
[b] n.d. = not determined.

butyryl side chains.

2.2. Determinations of density

Density measurements were performed on 0.5 mm thick hot-melt pressed films produced according to a method described by Nilsson et al. (Nilsson et al., 2022). After drying the films at 60 °C overnight, the dry densities of these films were determined by measuring the weight and dimensions. An external micrometer was used for thickness determination, and ImageJ, together with mm-paper, was used to determine the area. Wet density was determined by saturating the films in 35 °C water for 24 h and evaluating them similarly to the dry films after wiping the excess water off the films.

2.3. DVS and GAB model

The vapor sorption isotherms of CA, CAP, CABI, CABII, CABIII, and EC, were analyzed by DVS at 25 °C using a DVS resolution instrument (Surface Measurement System, London, UK). Samples weighing 10–80 mg were exposed to a series of RH between 0 and 80 %. The samples were pre-sieved before mounting them in the balance, and the RH was decreased from 20 to 0 % and cycled from 0 to 80 % in 10 % steps. The minimum waiting time was set to 40 min with a condition for the slope to go below 0.002 % during the last 30 min for each step before the next humidity step was started. The resulting isotherm was plotted against the RH steps and investigated with the GAB model. To retrieve the parameters m_0, K, and C in eq. 1, polynomial regression of the DVS data was performed according to Eq. (2):

$$\frac{a_w}{w} = a + ba_w + ca_w^2 \tag{2}$$

where a_w is the water activity, w is the dry basis moisture content, b and c are the solutions to the following equations along with m_0, which uses a and b. (Blahovec & Yanniotis, 2008, 2010):

$$aK^2 + bK + c = 0 \tag{2a}$$

$$C = \frac{b}{aK} + 2 \tag{2b}$$

$$m_0 = \frac{1}{(b + 2Ka)} \tag{2c}$$

Although the GAB equation, in many cases, accurately describes the sorption isotherm, it generally fails at higher water activities (Blahovec & Yanniotis, 2010). The experiments in this study will not exceed 80 % RH, and GAB was shown to be applicable for gas sorption in CA (Vopička & Friess, 2014).

2.4. Polymer modeling

The DS values for CA and CAP in Table 1 were used when constructing the CA model systems. CA and CAP were chosen as targets for the models since their water intake ratios are significantly different. The polymer chains were built using the Discovery Studio Visualizer 4.5 (BIOVIA, 2016). They consisted of three chains, each with 36 base monomer units and randomly distributed substituents. Be aware that in a real system the DS may not be fully random. CHARMM36 force field (Huang & MacKerell, 2013) was used for the model since it has been successfully used to predict starch's thermal and mechanical properties (Özeren et al., 2020a, b, 2021). TIP3P force field parameters were used for water atoms, which is recommended for CHARMM36 (Jorgensen et al., 1983). The hydrogen bonds of the polymers were constrained using the LINCS function (Hess et al., 1997) with the order of three. For a more detailed description, see the supplementary information Section 2. Simulation Details.

3. Results and discussion

The materials investigated have been analyzed in a previous study by Nilsson et al. where it was noted that CA absorbed the most water followed by EC, CABI, CAP, CABII, and CABIII (Nilsson et al., 2022). As the average side chain length increases, the material became less prone to absorb water, as also observed by Ong et al. (Ong et al., 2013). In addition, the T_g decreased with increasing average side chain length. Both observations could be explained by a progressively decreasing influence of hydrogen bonding as the average side chain length increased. These results collectively gave rise to two key questions: How was the water distributed in the samples? Did the water molecules interact with specific functional groups in the cellulose esters? To answer these questions, a combination of experiments and MD modeling was used.

3.1. Water interaction with esters – experimental part

3.1.1. Water interaction with esters characterized by DVS

The amount of water absorbed by the polymers at varying RH was determined by DVS, as displayed in Fig. 1. The DVS isotherms show that water absorption increases as RH increases. At most RH values, CA absorbed the most water, followed by CABI, CAP, EC, CABII, and CABIII. The 8 % water absorbed by CA at 80 % RH, measured in this study, corresponds to 9 % as reported by Gaudio et al. (Gaudio et al., 2021). Stiubianu et al. showed that CA, with a DS of 1.2, absorbed around 13 % water at 80 % RH, with a hysteresis effect evident from 20 % RH (Stiubianu et al., 2011). The trend in Fig. 1 agrees with earlier determinations of water uptake by submerged films, Table 1 (Nilsson et al., 2022). In literature, water absorption of 2.5 % at 80 % RH was reported for EC, which is slightly higher than the 2 % reported in this study. This difference could be related to a difference in DS values (Li et al., 2015). The desorption (the dashed lines in Fig. 1) decreased with decreasing RH, but the absorption and desorption did not follow the same pattern, giving rise to a hysteresis effect, which is more clearly shown in Fig. 2, presented as the difference in mass between absorption and desorption.

The isotherms, displayed in Fig. 1, indicate that CA and EC exhibit hysteresis effects, while the other polymers showed less change in water absorption/desorption at different RHs. Fig. 2 shows that the largest difference in absorption and desorption amongst CAP, CABI, CABII, and CABIII occurs between 60 % RH and 70 % RH. The shape of the CA curve

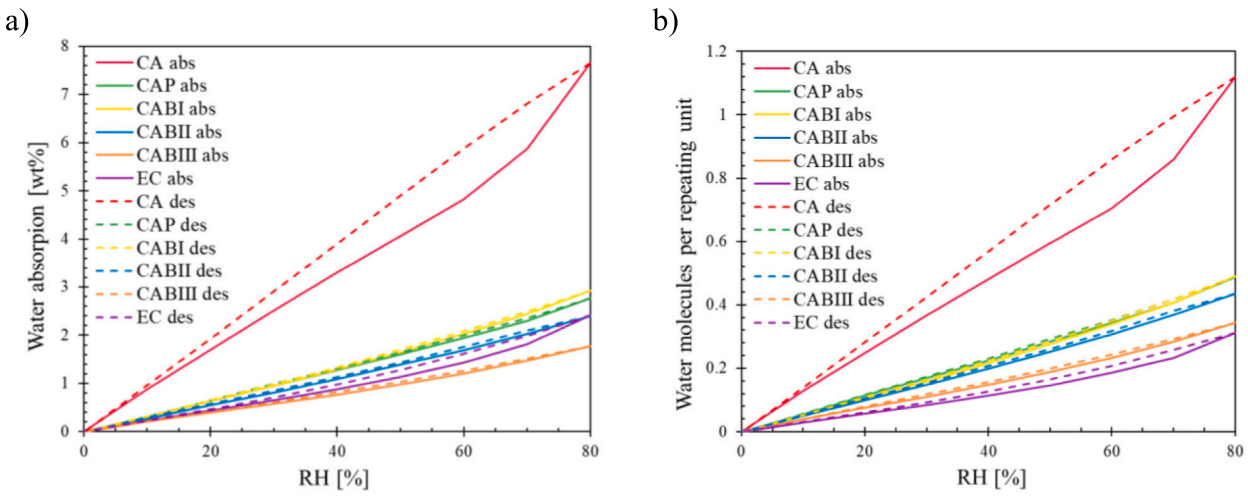

Fig. 1. a) Equilibrium data from DVS measurements for CA, CAP, CABI, CABII, CABIII, and EC. Absorption and desorption were performed in steps of 10 between 0 and 80 % RH, b) The number of water molecules per repeating unit for each DVS step for the same materials.

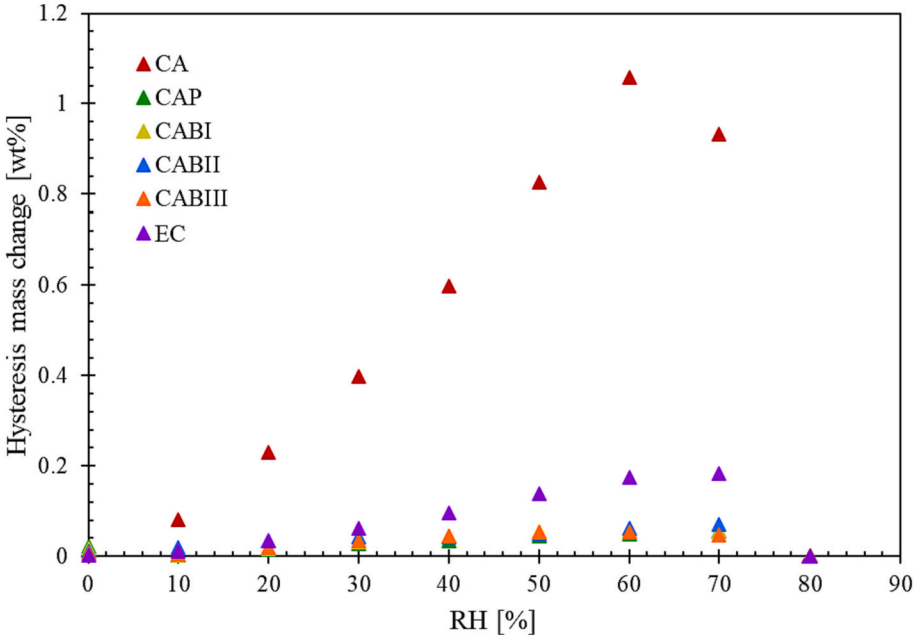

Fig. 2. The hysteresis in weight difference between absorption and desorption at different humidities for CA, CAP, CABI, CABII, CABIII, and EC.

in Fig. 2 is similar to that of aged CA, reported by Gaudio et al. (Gaudio et al., 2021). In the literature, one reason for the hysteresis effects of bio-based polymers, like oxidized cellulose, is the induction of deformation of the polymeric structure by water, shown by a decrease in storage modulus (Salmén & Larsson, 2018). If deformation of the polymeric structure was the reason for the sudden increase at 60 % RH for CA, then it is interesting that the addition of only one extra methyl group on the acetate, i.e. going from CA to CAP, or the addition of only a small number of substituents with two methyl groups, i.e. going from CA to CABI, was enough to remove the driving force for this water-induced deformation.

Since the cellulose esters investigated in this study were selected for having a similar total DS, the number of hydrogen bonding sites was approximately equal. It was therefore assumed that the number of water molecules per repeating unit was equal. Consequently, the water absorbed at different RH was normalized to the molar mass of the average repeating unit, see Fig. 1b. Calculations for these can be found in SI. The extension of the average chain lengths reduced the absorbed water molecules per repeating unit from 1.12 for CA to 0.34 for CABIII at 80 % RH. This agrees with a previous paper (Nilsson et al., 2022), where the difference in water interactions between CA, CAP, and CAB was attributed to the screening of hydrogen bonds by the average side chain length, making it more difficult for water molecules to locate the hydrogen bonding sites in the central parts of the cellulose chain. EC also exhibited a larger hysteresis effect than CAP and CABIII. Compared to CA, 0.31 water molecules per repeating unit of EC seems to be enough to deform its structure, causing hysteresis and highlighting the water-sensitive nature of EC.

Furthermore, for CA, Fig. 1b shows that 0.7 water molecules per repeating unit appears to be a critical number. Above this critical number, the absorption per humidity step increases more than below the critical number. The increased water absorption above 0.7 water molecules per repeating unit could mean that the maximum number of attractive sites to interact on each molecule is on average 0.7 sites. Any

water content above that may not directly interact with CA and instead undergo cluster formation. Another interpretation could be that 0.7 water molecules per repeating unit is the limit at which intermolecular attraction between CA chains are interrupted or sufficiently screened to allow movement of the molecular structure, allowing more water to enter per humidity step. To investigate this further, the DVS data was fitted to the GAB model and MD simulations were performed to confirm if water forms more and larger clusters.

3.1.2. Fitting the DVS data to the GAB model

Fig. 3 shows the fitting of the GAB model to the DVS data and Table 2 shows the different GAB parameters and how well the model fits the data. The table shows that the GAB equation well fits the CABI to EC data, while it fits less for the CA and CAP, with R^2 of 0.79 and 0.88, respectively. The C parameter for all materials is above 2, which means that they follow a sigmoidal curve with an inflection point, i.e., type II absorption according to Brunauer's classification. The K parameter lies between 0 and 1, which fulfills the model criteria for that parameter. The m_0 parameter represents the amount of water at which all water binding sites are occupied in a monolayer, which means that for CA, the water absorbed beyond 4.3 wt% was more than the available sites and was therefore expected to form clusters. This value is close to the point of abrupt increase in Fig. 1a at 4.8 wt%, indicating that the cause of this increase in water sorption was cluster formation. The monolayer limit, m_0, declines in the order of CA, CAP, CABI, CABII, CABIII, and EC, which follows a similar trend to total water absorption, Table 1. Assuming that passing the point of m_0 for CA creates the hysteresis, the other materials, except EC, should not have an m_0 limit within the studied range of RH. The GAB model appears useful for CA but for the other esters the positioning or existence of m_0 seems to not correlate to any observable changes in the sorption isotherms, Fig. 1. The GAB parameters have previously been reported to be useful for calculating mean cluster size (Alipour et al., 2019) but surprisingly, our calculations showed no

Table 2
GAB parameters m_0, C, and K for each material together with the R^2 of the polynomial fit of Eq. (2) to the sorption data.

	m_0	C	K	R^2
CA	4.26	3.74	0.52	0.790
CAP	3.61	2.06	1.00	0.877
CABI	2.95	2.07	0.81	0.998
CABII	2.58	2.14	0.85	0.993
CABIII	1.13	3.00	0.57	0.984
EC	1.01	3.75	0.46	0.996

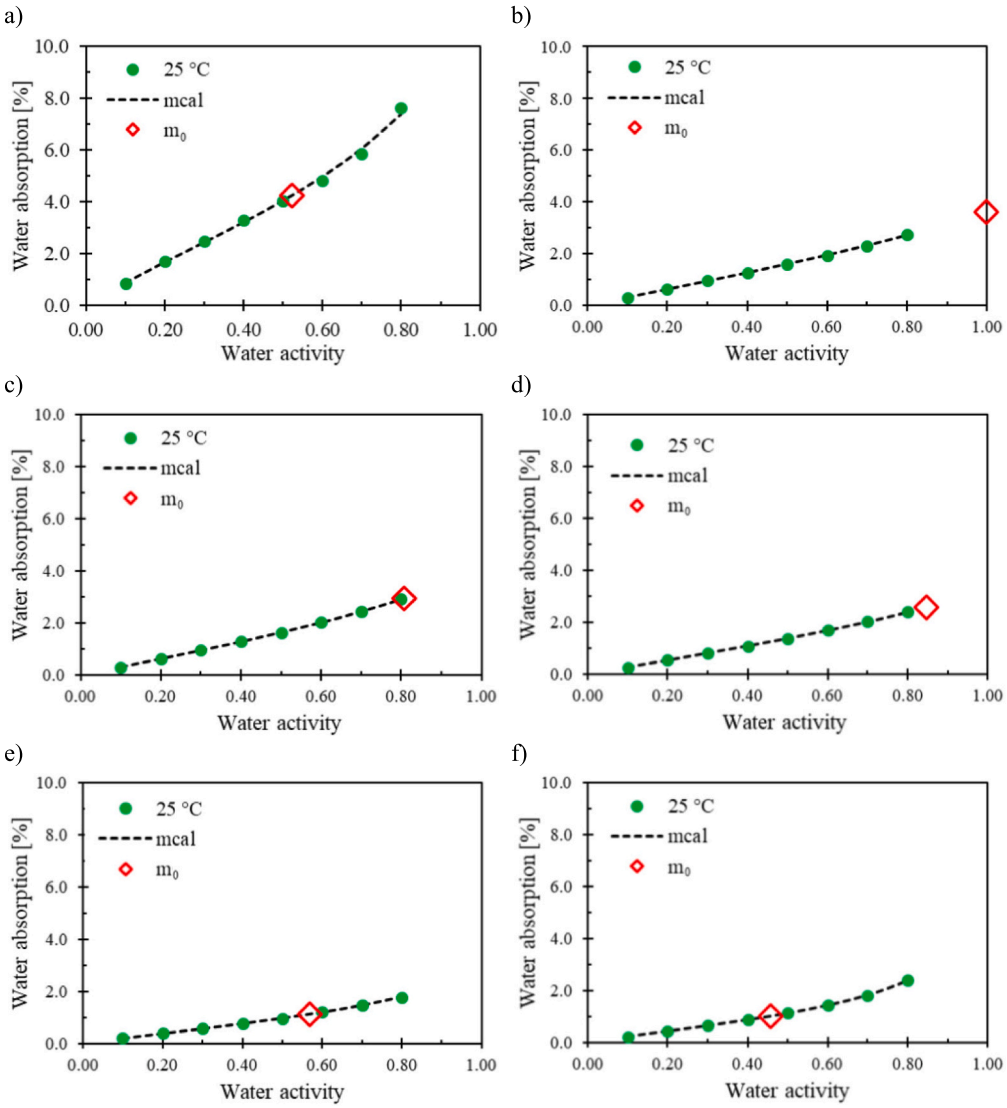

Fig. 3. DVS sorption isotherms over water activity, calculated GAB isotherms (mcal), and mass of water for one monolayer (m_0) for a) CA, b) CAP, c) CABI, d) CABII, e) CABIII, and f) EC.

clustering for CA. These contradictory results regarding clustering motivated MD simulations of CA and CAP at 0, 40, and 80 % RH.

3.1.3. Reason for the hysteresis

The hysteresis curve for CA shows that, above 60 % RH, the increase in water absorption becomes progressively larger, i.e., a larger step occurs between 70 and 80 % RH than 60 to 70 % RH. This could be explained by the fact that enough water is absorbed at 60 % RH to decrease the T_g, causing the chains to move more easily and allowing clusters of water molecules to form. The effect of moisture on the T_g is generally challenging to investigate experimentally because the T_g of CA is 193 °C, i.e., well above the boiling point of water and the encapsulation of water causes experimental problems. Upon desorption, at 80 to 70 % RH, the isotherm does not follow the absorption isotherm. Instead, the desorption curve decreases more linearly. This could be attributed to deformation upon absorption, which creates a state of higher polymer conformation entropy and lower polymer-polymer interactions. At this first desorption step, 80 to 70 % RH, the water molecules that are not strongly interacting with the polymer are speculated to desorb first. The prior structural changes of the system during absorption resulted in the polymer chains moving to accommodate more water, thereby creating a new system. This results in a system that needs to rearrange again during desorption. However, since the polymer structures beginning at 60 % RH (before further absorption) and beginning at 80 % RH (before desorption) were different from each other, it is plausible that the polymer structures at 70 % RH after absorption and desorption, respectively, were also different. The mobility of the CAP and CABI-III is likely larger than CA due to their lower T_g but, simultaneously, the amount of water absorbed by CAP and CABI-III was lower since the longer average side chains screen the hydrogen bonding sites. This results in their structures not accommodating as much water, thus not rearranging the polymer chains in the same way as CA and not causing hysteresis.

3.2. Water interaction with esters – simulations

The experimental section implies that (i) the hysteresis seems to be caused by the deformation of the polymer chains, and (ii) the absorbed water molecules may form clusters even below one water molecule per repeating unit. The deformation likely depends on the amount of water absorbed and its plasticizing effect on the polymers, related to a decrease in T_g. This decrease in T_g is expected to be more prominent when there is a more significant hysteresis effect. The MD simulations were performed on CA and CAP to confirm the implications of the experimental results (i) and(ii), where CA clearly showed a hysteresis effect whereas CAP did not. In the simulated CAP system, there were six residual OH groups per chain. In order to keep the atomistic net charges at zero, the terminal units of the chains were kept unmodified. Consequently, these OH groups had to be placed three by three at the two repeating units at the chain ends. To be able to compare the results, six OH groups were placed in a similar manner in CA, where the remaining residual 15 OH groups were randomly positioned along the chain. There was no more than one OH group per repeating unit.

3.2.1. PVT curves

The PVT curves for CA and CAP in dry and 80 % RH conditions, which can be found in SI Fig. S1-S4, were used to calculate the T_g presented in Table 3. The experimentally determined T_g for the dry materials were similar but note that there have been challenges involved in determining T_g from computed PVT data (Özeren et al., 2020a, b). The rate at which the changes in temperature occur in MD simulations are by necessity much higher than in experiments. This effect leads to a higher T_g in simulations. On the other hand, the finite chain length in simulations leads to a larger number of chain ends than in the real system. This leads to a lower T_g in simulations than in experiments. The effect that dominates depends on the system, type of polymer (chemistry, molecular weight, etc.), presence of other molecules (like water), and size of the MD system. Another observation, which is logical considering the difference in water uptake, was that the simulated wet and dry CAP had similar T_g, whereas CA showed clear changes in the PVT graphs and, therefore, T_g. The experimentally determined dry and wet densities for CA and CAP, Table 3, were fully predicted by the MD simulations with a maximum difference of 3 % between simulations and experiments.

Table 3
Experimental and simulated T_g at 0 % RH (dry) and 80 % RH. Densities for oven-dried and wet (submerged in water) hot-melt pressed films (experimental) and simulated 0 % RH (dry) and 80 % RH for CA and CAP.

Polymer	Experimental dry	Experimental wet	Simulated dry	Simulated 80 % RH
T_g CA [°C]	193 ± 1	n.a.	214 ± 5	180 ± 10
T_g CAP [°C]	141 ± 1	n.a.	129 ± 10	125 ± 10
Density CA [g cm^{-3}]	1.22 ± 0.01	1.26 ± 0.01	1.21 ± 0,01	1.24 ± 0.02
Density CAP [g cm^{-3}]	1.17 ± 0.03	1.20 ± 0.02	1.14 ± 0.03	1.16 ± 0.04

When wetted, both the simulated and experimental density increased, Table 3, indicating that water entered empty spaces in the structure rather than causing swelling. At the same time, more water was absorbed (12 % experimentally for CA, Table 1) than the increase in density (<4 %). This implies that swelling also occurs. The simulated wet system, i.e. the system with the polymers exposed to 80 % RH, showed a decrease in T_g of 30 °C for CA and 10 °C for CAP. Water cannot exist practically in a system at those temperatures, so the wet values are theoretical and challenging to prove experimentally. Nevertheless, this shows that the thermal properties of CA are affected by water and, given that the thermal properties depend on the structure, this can explain the deformation that causes hysteresis. T_g depends on intermolecular interactions, especially hydrogen bonding, as discussed in Section 3.1, which means that when water absorbs into the structure, it breaks intermolecular hydrogen bonds to a certain degree, which in turn decreases the T_g. CAP, which has a lower water interaction and absorption, also shows a decrease in T_g in wet conditions, meaning that despite its more hydrophobic nature, due to the propionyl compared to acetyl, a relatively small amount of water molecules interpose themselves between chains, decreasing the hydrogen bonding between the polymer chains.

3.2.2. Intramolecular hydrogen bonding distances of CA and CAP

Fig. 4 shows the radial distribution function (RDF) of interactions within a polymer chain between O2-O6 and O3-O5 for CA and CAP systems at RH values of 0, 40, and 80 %. The intrachain interactions in the cellulose esters are similar to the unsubstituted crystalline regenerated Cellulose II structure, shown by WAXS measurements by Nilsson et al. (Nilsson et al., 2022). Cellulose II is more thermodynamically stable than Cellulose I, the most common form of cellulose in nature. This similarity to Cellulose II structure may be noted since the simulations strive for the most thermodynamically stable form.

The first peak of O3-O5 is broad, indicating the distance between the O3 of one repeating unit and the O5 of the neighboring connected repeating unit. The narrowness of the second peak indicates that it is on the same repeating unit and will thus always have one distance. The O3-O5 intramolecular distances were unaffected by the moisture, both for CA and CAP. However, for O2-O6 there is a shift of the peak from 3 Å to 2.5 Å for CA as the RH increases. In contrast, the simulations for CAP displayed no interaction peak at 2.5 nor 3 Å. This could be because the substituents in CAP are bulkier, thus the O6 would be more likely to phase away from the backbone, with broader signals around 5 Å. It should be noted that the water content for CAP at 80 % RH and CA at 40 % RH were around 3 % for both. A small increase in the distance around 2.5–4 Å was noticeable for CAP compared to CA, probably due to an increase in the average side chain lengths. The largest peak for O2-O6, at

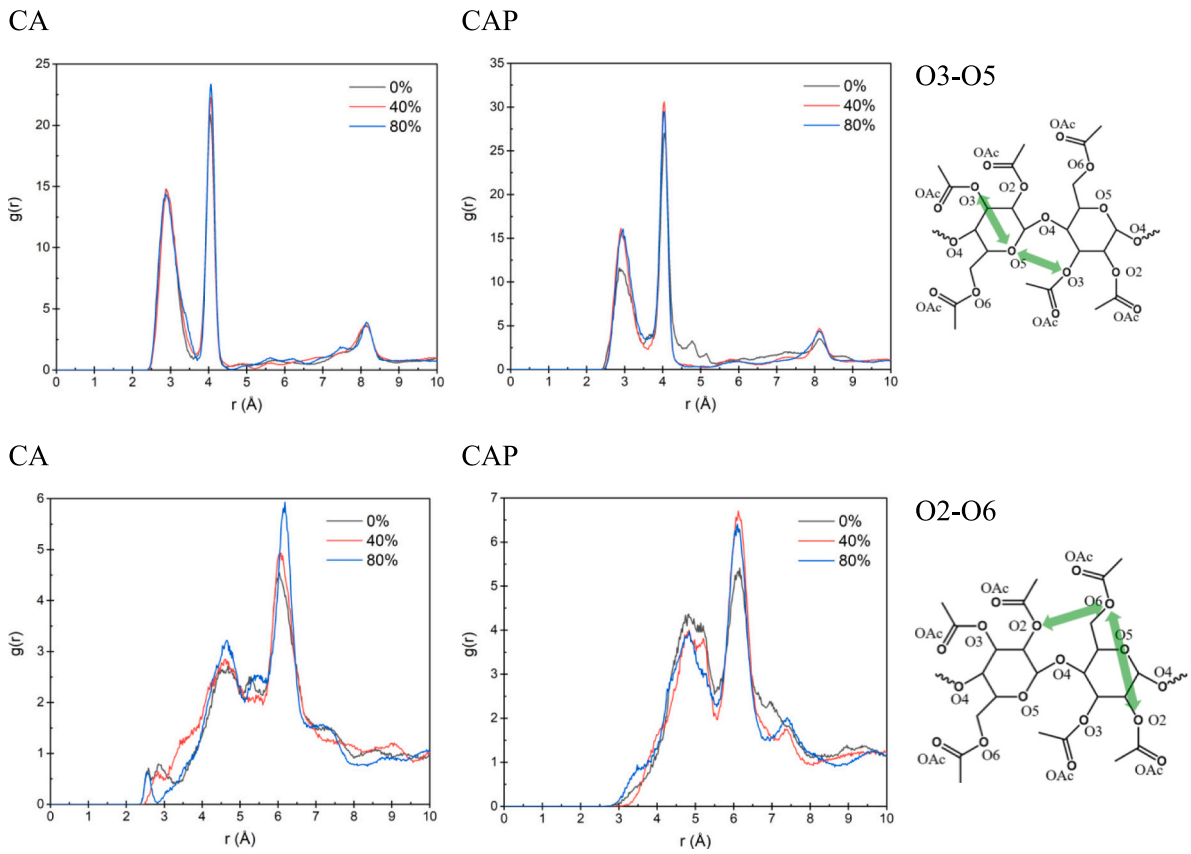

Fig. 4. Comparison of intra-RDF of CA's and CAP's O3-O5 and O2-O6, with the main intramolecular distances displayed in the chemical structure to the right. The molecular images on the right side are for illustration purposes and do not represent systems with the correct DS values.

6 Å, appears to increase slightly for both CA and CAP when exposed to water, possibly due to increased relaxation of the chains when the amount of water increases. To conclude, CA showed larger changes, such as the shift for O2-O6, indicating that water affects CA and CAP to a similar extent but in a different way. It is likely that both the length of the ester groups and the different amounts of residual OH group contribute to the differences observed between CA and CAP.

Intra-RDF was also investigated for the acetyl and propionyl carbonyl oxygen related to the different oxygens in the structure, O2, O3, O4, O5, and O6, Fig. 5. For CA, the peak at 3 Å increases from 0 % to 40 % RH and slightly more for 80 % RH, which indicates that the closest acetyl carbonyl oxygen reconfigures closer to the O4 oxygen. The reason why this occurs when water is present is unclear. In comparison, there is no observed change for CAP at 3 Å. Note that the CAP plot in Fig. 5 includes both acetyl and propionyl carbonyl oxygen but no effect of the acetyl fraction is observed. The carbonyl oxygen distances to the other mentioned oxygens did not change for CAP nor CA. The other intra-RDF plots can be found in SI Fig. S5-S8.

3.2.3. *Water coordination to the polymer chains*

How the structure is affected by water depends on how water coordinates with itself but also to the polymer's functional groups. From

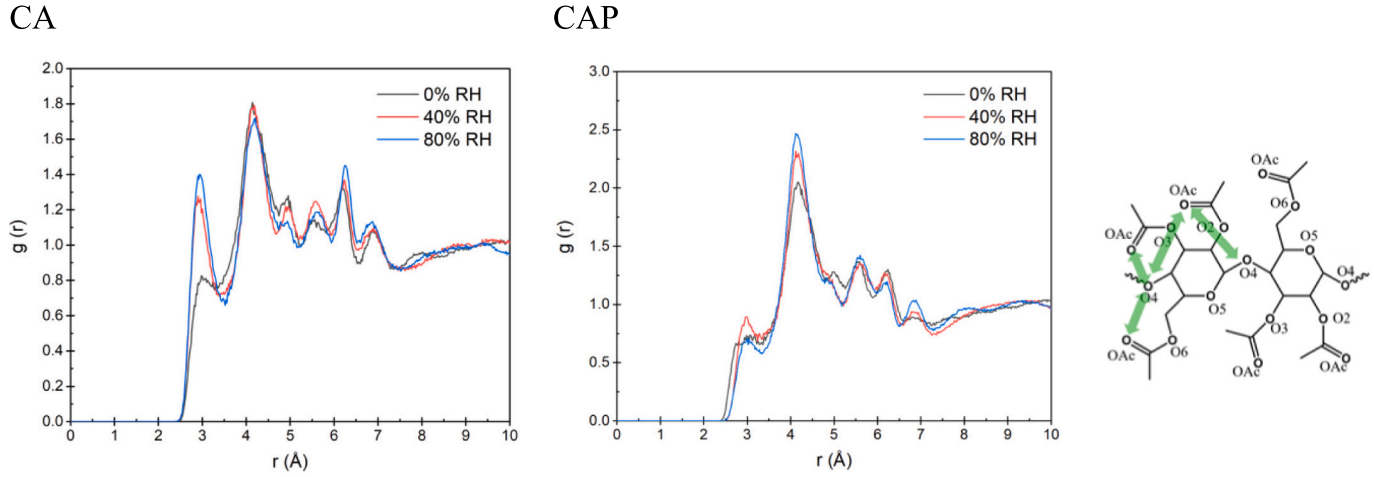

Fig. 5. Intra-RDF of CA's and CAP's carbonyl oxygen to O4, with the main intramolecular distances displayed in the chemical structure to the right. The molecular image on the right side is for illustration purposes and does not represent a system with the correct DS values.

the intramolecular distance discussed, it is evident that water did not induce big changes in the distance between different oxygens within the polymer structure, except for the acetyl carbonyl oxygen distance to the O4. This indicates that water interacts with the carbonyl oxygen of acetyl. The way water coordinates with different oxygens in the polymer is shown by the RDF curves in Fig. 6. It is clearly visible that, for CA, the water molecules surround the carbonyl oxygen in the acetyl group at both 40 % and 80 % RH at around a distance of 2 Å. This was expected since the carbonyl oxygen in the acetyl group is the outermost oxygen from the view of the backbone and is therefore the most probable interaction site for water.

Peaks from the carbonyl oxygen of acetyl and propionyl also appear at 2 Å for CAP. CAP has a DS of 2.64 for propionyl and a DS of 0.21 for acetyl, meaning that the majority of O2, O3, and O6 in CAP is connected to a propionyl group. Therefore, it is interesting to observe that water preferentially interacts with the carbonyl oxygen of the acetyl group. When the humidity was increased to 80 % RH, there was a similar amount of water coordinating with the acetyl and propionyl carbonyl oxygen, indicating that the acetyl carbonyl sites were saturated, therefore water starts to coordinate with the carbonyl oxygen of the propionyl groups instead.

Moreover, hydroxyl groups are often recognized as a strong group for hydrogen bonding. For CAP, there was a strong coordination of water with the acetyl carbonyl oxygen, which comprises 7 % of the side chains in CAP, whereas the OH groups comprise 5 % for CAP and 20 % for CA. If the water interactions with the residual OH groups had been strong, strong signals of water coordinating to O2, O3, or O6 at 2 Å would have been obtained. Following the observation of acetyl in CAP, it is hypothesized that the origin of the O6 peak in CA could be due to an OH group at O6, or an OH group close to O6, that interacts with the water molecules. However, the peak is relatively small in comparison to the carbonyl oxygen belonging to acetyl and propionyl. The simulation thus suggests that water does not coordinate significantly with the residual hydroxyl groups in the cellulose ester samples. The reason for this could be that the amount of OH compared to acetyl and propionyl is low enough to be obstructed by the longer and bulkier structure of acetyl and propionyl, preventing water from getting close enough to OH for hydrogen bonding.

The first peak distances (1.9–2.0 Å) for all the systems suggest that they create strong hydrogen bonds with the polymer. Jeffrey categorized hydrogen bonds in proteins at 0–2.5 Å as strong, 2.5–3.2 Å as moderate, and 3.2–4 Å as weak (Jeffrey, 1997). The peak intensity at 40 % RH is higher than at 80 % RH, indicating that water molecules could disrupt each other in the systems at higher RH. Therefore, the clustering probability of water molecules was analyzed at 40 and 80 % RH and is presented in Fig. 7. Both CA and CAP showed a probability of clustering at 40 % RH. Interestingly, clustering occurred well below the GAP calculated m_0 value for both CA and CAP. The probability of forming larger clusters increased when RH was increased from 40 % to 80 % for both CA and CAP. The majority of water molecules were single, which could have been due to insufficient simulation time to enable more clusters. However, the simulations also indicated that water molecules tend to create larger clusters (four molecules or higher in this case) at higher RH, as expected. The probability of four and more water molecules per cluster is higher for CA than for CAP, which supports the higher water absorption of CA and confirms that the hysteresis effect could be from water cluster formation. As mentioned, due to limited simulation time, not too much emphasis can be placed on the cluster probability. In

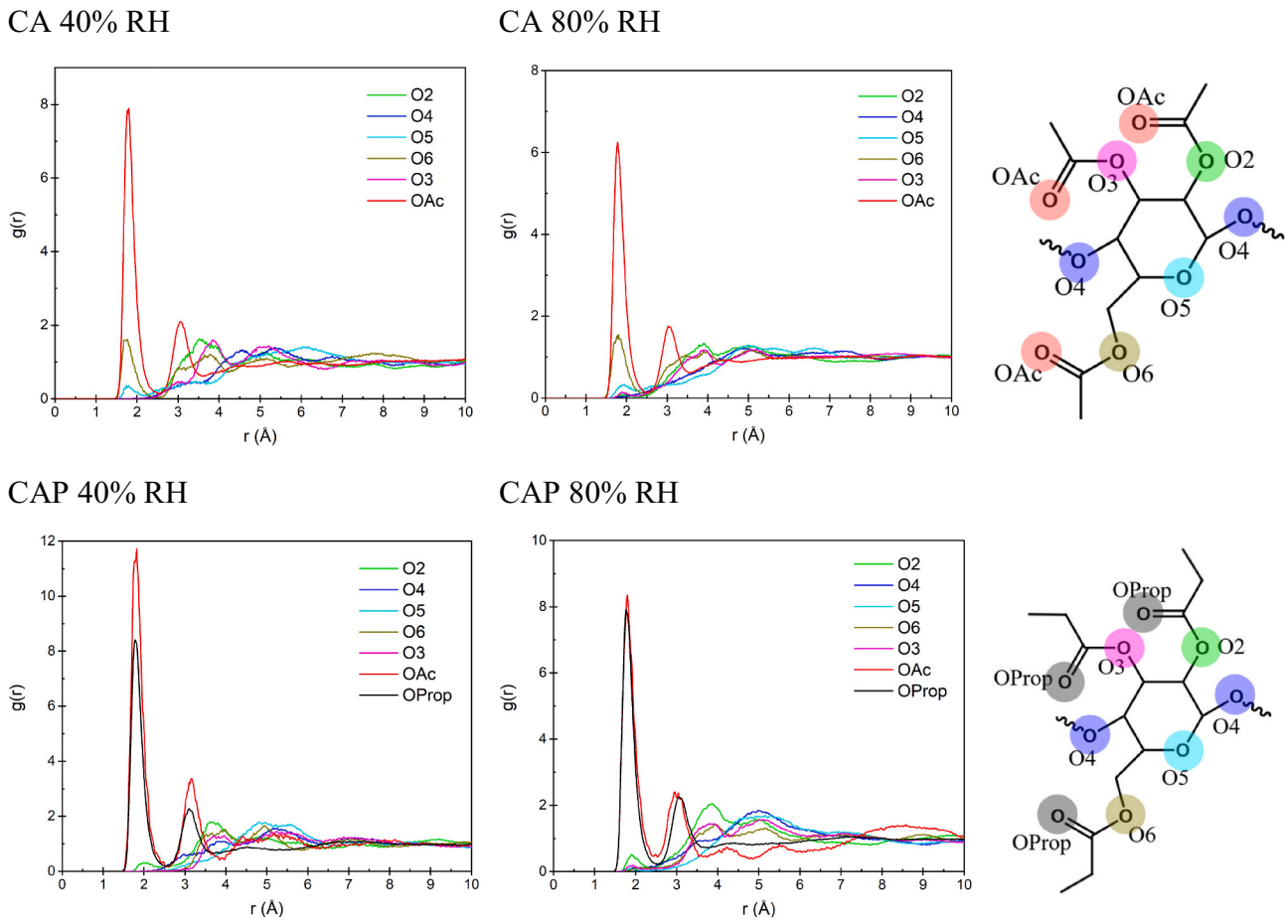

Fig. 6. Intra-RDF of CA's and CAP's oxygens with water's hydrogens at 40 % RH and 80 % RH. The oxygen position numbers are clarified in the chemical structure to the right. The molecular image on the right side is for illustration purposes and does not represent a system with the correct DS values.

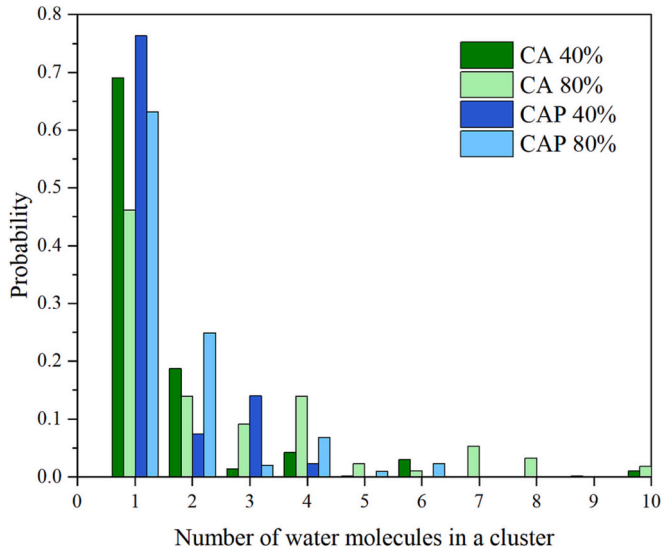

Fig. 7. The density probability of the number of water molecules in a cluster in the systems.

summary, the simulations answer how water is oriented in the materials and which functional groups water coordinates to.

4. Conclusion

This study used a dual experimental and theoretical approach to investigate polymer-water interactions. It has been demonstrated that, for CA, there is a crucial number of water molecules per repeating unit above which absorption increases drastically due to water interacting with hydrogen bonding sites. This prevents polymer-polymer hydrogen bonding and increases chain flexibility, allowing more water to absorb. Upon exposure to water, the intramolecular distances between oxygens changed only slightly for CA and even less for CAP, indicating that the effects of water absorption do not considerably change polymer conformation. Consequently, changes in density, for example, have instead been attributed to intermolecular changes. Although clusters can be formed at higher humidities, the GAB model suggested that no clustering occurred for any of the studied materials in the investigated humidity range (0 to 80 % RH). The MD simulations, on the other hand, have indicated a probability of water clustering for both CA and CAP from 40 % RH, with CA being more likely to form larger clusters. The probability of forming larger clusters increased more for CA than for CAP as humidity increased from 40 to 80 % RH. Surprisingly, the simulations shown that water coordinates more strongly to the carbonyl group of the acetyl than OH groups. This reveals that average side chain length is a critical factor in cellulose esters' interactions with water at different RH.

CRediT authorship contribution statement

Robin Nilsson: Conceptualization, Methodology, Validation, Formal analysis, Investigation, Resources, Data curation, Writing – original draft, Writing – review & editing, Visualization. **Hüsamettin Deniz Özeren:** Methodology, Validation, Formal analysis, Investigation, Writing – original draft, Writing – review & editing, Visualization. **Okky Dwichandra Putra:** Methodology, Formal analysis, Writing – review & editing, Supervision. **Mikael Hedenqvist:** Methodology, Formal analysis, Writing – review & editing, Supervision. **Anette Larsson:** Conceptualization, Methodology, Formal analysis, Resources, Data curation, Writing – original draft, Writing – review & editing, Supervision, Project administration, Funding acquisition.

Declaration of competing interest

The authors declare that they have no known competing financial interests or personal relationships that could have influenced the work reported in this paper.

Data availability

Data will be made available on request.

Acknowledgements

This project was partially financed by Formas, 2017-00648, and is associated with Treesearch, BIOINNOVATION, VINNOVA, Sweden and FibRe – Design for circularity – Lignocellulose-based thermoplastics, a VINNOVA competence center. Computing (SNIC) at KEBNEKAISE was partially financed by the Swedish Research Council through grant agreement number SNIC 2021/5–266.

Appendix A. Supplementary information

Supplementary data to this article can be found online at https://doi.org/10.1016/j.carbpol.2023.120616.

References

Agrawal, A. M., Manek, R. V., Kolling, W. M., & Neau, S. H. (2004). Water distribution studies within microcrystalline cellulose and chitosan using differential scanning calorimetry and dynamic vapor sorption analysis. *Journal of Pharmaceutical Sciences, 93*(7), 1766–1779. https://doi.org/10.1002/jps.20085

Alamri, M. S., Mohamed, A. A., Hussain, S., Ibraheem, M. A., & Abdo Qasem, A. A. (2018). Determination of moisture sorption isotherm of crosslinked millet flour and oxirane using GAB and BET. *Journal of Chemistry, 2018*. https://doi.org/10.1155/2018/2369762

Alipour, N., Vinnerås, B., Gouanvé, F., Espuche, E., & Hedenqvist, M. S. (2019). A protein-based material from a new approach using whole defatted larvae, and its interaction with moisture. *Polymers, 11*(2), 1–13. https://doi.org/10.3390/polym11020287

Arslan, N., & Toğrul, H. (2006). The fitting of various models to water sorption isotherms of tea stored in a chamber under controlled temperature and humidity. *Journal of Stored Products Research, 42*(2), 112–135. https://doi.org/10.1016/j.jspr.2005.01.001

Asai, T., Taniguchi, H., Kinoshita, E., & Nakamura, K. (2001). Thermal and mechanical properties of cellulose acetates with various degrees of acetylation in dry and wet states. In *, 275–280. Recent advances in environmentally compatible polymers*. https://doi.org/10.1533/9781845693749.5.275

Bergenstråhle, M., Wohlert, J., Himmel, M. E., & Brady, J. W. (2010). Simulation studies of the insolubility of cellulose. *Carbohydrate Research, 345*(14), 2060–2066. https://doi.org/10.1016/j.carres.2010.06.017

BIOVIA, BIOVA Materials Studio, Release 2016 San Diego: Dassault Systèmes, 2016.

Blahovec, J., & Yanniotis, S. (2008). Gab generalized equation for sorption phenomena. *Food and Bioprocess Technology, 1*(1), 82–90. https://doi.org/10.1007/s11947-007-0012-3

Blahovec, J., & Yanniotis, S. (2010). "Gab" generalised equation as a basis for sorption spectral analysis. *Czech Journal of Food Sciences, 28*(5), 345–354. https://doi.org/10.17221/146/2009-cjfs

Bratasz, Kozłowska, A., & Kozłowski, R. (2012). Analysis of water adsorption by wood using the Guggenheim-Anderson-de Boer equation. *European Journal of Wood and Wood Products, 70*(4), 445–451. https://doi.org/10.1007/s00107-011-0571-x

Brunauer, S., Demin, S. L., Demin, W. E., & Teller, E. (1940). On a theory of the van der Waals adsorption of gases. *Journal of the American Chemical Society, 62*(7), 1723–1732. https://doi.org/10.1021/ja01864a025

del Gaudio, I., Hunter-Sellars, E., Parkin, I. P., Williams, D., Da Ros, S., & Curran, K. (2021). Water sorption and diffusion in cellulose acetate: The effect of plasticisers. *Carbohydrate Polymers, 267*(January), Article 118185. https://doi.org/10.1016/j.carbpol.2021.118185

Driemeier, C., Mendes, F. M., & Oliveira, M. M. (2012). Dynamic vapor sorption and thermoporometry to probe water in celluloses. *Cellulose, 19*(4), 1051–1063. https://doi.org/10.1007/s10570-012-9727-z

Gabor (Naiaretti), D., & Titia, O. (2012). Biopolymers used in food packaging: A review. *Acta Universitatis Cibiniensis Series E: Food Technology, XVI*(2), 3–19.

Gårdebjer, S., Larsson, A., Löfgren, C., & Ström, A. (2014). Controlling water permeability of composite films of polylactide acid, cellulose, and xyloglucan. *Journal of Applied Polymer Science, 132*(1), 1–8. https://doi.org/10.1002/app.41219

Hatakeyama, H., & Hatakeyama, T. (1998). Interaction between water and hydrophilic polymers. *Thermochimica Acta, 308*(1–2), 3–22. https://doi.org/10.1016/s0040-6031(97)00325-0

Hess, B., Bekker, H., Berendsen, H. J. C., & Fraaije, J. G. E. M. (1997). LINCS: A linear constraint solver for molecular simulations. *Journal of Computational Chemistry, 18* (12), 1463–1472. https://doi.org/10.1002/(SICI)1096-987X(199709)18:12<1463::AID-JCC4>3.0.CO;2-H

Huang, J., & MacKerell, A. (2013). CHARMM36 all-atom additive protein force field: Validation based on comparison to NMR data. *Journal of Computational Chemistry, 2013*(34), 2135–2145. https://doi.org/10.1002/jcc.23354

Jeffrey, G. A. (1997). *An introduction to hydrogen bonding*. Oxford University Press. https://books.google.se/books?id=ZRAFifo37QsC.

Jorgensen, W. L., Chandrasekhar, J., Madura, J. D., Impey, R. W., & Klein, M. L. (1983). Comparison of simple potential functions for simulating liquid water. *The Journal of Chemical Physics, 79*(2), 926–935. https://doi.org/10.1063/1.445869

Keely, M. (2003). *Journal of Molecular Structure, 355*(1995), 33–46, 355, 1–14. papers2://publication/uuid/174CC5B6-05C4-4341-9B16-8A4061BBA7AA.

Klemm, D., Heublein, B., Fink, H. P., & Bohn, A. (2005). Cellulose: Fascinating biopolymer and sustainable raw material. *Angewandte Chemie - International Edition, 44*(22), 3358–3393. https://doi.org/10.1002/anie.200460587

Li, X., Jiang, F., Ni, X., Yan, W., Fang, Y., Corke, H., & Xiao, M. (2015). Preparation and characterization of konjac glucomannan and ethyl cellulose blend films. *Food Hydrocolloids, 44*, 229–236. https://doi.org/10.1016/j.foodhyd.2014.09.027

Lonsdale, H. K., Merten, U., & Riley, R. L. (1965). Transport properties of cellulose acetate osmotic membranes. *Journal of Applied Polymer Science, 9*(4), 1341–1362. https://doi.org/10.1002/app.1965.070090413

Lopez-Silva, M., Agama-Acevedo, E., Bello-Perez, L. A., & Alvarez-Ramirez, J. (2021). Influence of gelatinization degree and octenyl succinic anhydride esterification on the water sorption characteristics of corn starch. *Carbohydrate Polymers, 270*(May), Article 118378. https://doi.org/10.1016/j.carbpol.2021.118378

Mosquera-Giraldo, L. I., Borca, C. H., Parker, A. S., Dong, Y., Edgar, K. J., Beaudoin, S. P., Slipchenko, L. V., & Taylor, L. S. (2018). Crystallization inhibition properties of cellulose esters and ethers for a group of chemically diverse drugs: Experimental and computational insight. *Biomacromolecules, 19*(12), 4593–4606. https://doi.org/10.1021/acs.biomac.8b01280

Nilsson, R., Olsson, M., Westman, G., Matic, A., & Larsson, A. (2022). Screening of hydrogen bonds in modified cellulose acetates with alkyl chain substitutions. *Carbohydrate Polymers, 285*(November 2021), Article 119188. https://doi.org/10.1016/j.carbpol.2022.119188

Ong, R. C., Chung, T. S., Helmer, B. J., & De Wit, J. S. (2012). Novel cellulose esters for forward osmosis membranes. *Industrial and Engineering Chemistry Research, 51*(49), 16135–16145. https://doi.org/10.1021/ie302654h

Ong, R. C., Chung, T. S., Helmer, B. J., & De Wit, J. S. (2013). Characteristics of water and salt transport, free volume and their relationship with the functional groups of novel cellulose esters. *Polymer, 54*(17), 4560–4569. https://doi.org/10.1016/j.polymer.2013.06.043

Özeren, H. D., Guivier, M., Olsson, R. T., Nilsson, F., & Hedenqvist, M. S. (2020). Ranking plasticizers for polymers with atomistic simulations: PVT, mechanical properties, and the role of hydrogen bonding in thermoplastic starch. In *, Vol. 2. ACS Applied Polymer Materials* (pp. 2016–2026). https://doi.org/10.1021/acsapm.0c00191. Issue 5.

Özeren, H. D., Nilsson, F., Olsson, R. T., & Hedenqvist, M. S. (2021). Prediction of real tensile properties using extrapolations from atomistic simulations; an assessment on thermoplastic starch. In *, Vol. 228. Polymer*. https://doi.org/10.1016/j.polymer.2021.123919

Özeren, H. D., Olsson, R. T., Nilsson, F., & Hedenqvist, M. S. (2020). Prediction of plasticization in a real biopolymer system (starch) using molecular dynamics simulations. *Materials & Design, 187*, Article 108387. https://doi.org/10.1016/j.matdes.2019.108387

Palin, M. J., Gittens, G. J., & Porter, G. B. (1975). Determination of diffusion coefficients of water in cellulose acetate membranes. *Journal of Applied Polymer Science, 19*(4), 1135–1146. https://doi.org/10.1002/app.1975.070190421

Qiao, Z., Wang, Z., Zhang, C., Yuan, S., Zhu, Y., & Wang, J. (2012). PVAm–PIP/PS composite membrane with high performance for CO2/N2 separation. *AIChE Journal, 59*(4), 215–228. https://doi.org/10.1002/aic

Rajabnezhad, S., Ghafourian, T., Rajabi-Siahboomi, A., Missaghi, S., Naderi, M., Salvage, J. P., & Nokhodchi, A. (2020). Investigation of water vapour sorption mechanism of starch-based pharmaceutical excipients. *Carbohydrate Polymers, 238* (January), Article 116208. https://doi.org/10.1016/j.carbpol.2020.116208

Reid, D. S., & Levine, H. (1991). Beyond water activity: Recent advances based on an alternative approach to the assessment of food quality and safety. *Critical Reviews in Food Science and Nutrition, 30*(2–3), 115–360. https://doi.org/10.1080/10408399109527543

Roos, Y. H. (1995). Chapter 4 - Water and phase transitions. In Y. H. Roos (Ed.), *Phase transitions in foods* (pp. 73–107). Academic Press. https://doi.org/10.1016/B978-012595340-5/50004-3.

Salmén, L., & Larsson, P. A. (2018). On the origin of sorption hysteresis in cellulosic materials. *Carbohydrate Polymers, 182*(September 2017), 15–20. https://doi.org/10.1016/j.carbpol.2017.11.005

Schuetzenberger, P., & Dreyfus, H. (2016). In *CA cellulose acetate* (pp. 33–38). https://doi.org/10.1016/B978-1-895198-92-8.50012-4

Simon, M., Fulchiron, R., & Gouanve, F. (2021). *Experimental and modelling studies of water sorption properties of cellulosic derivative fibers*. https://doi.org/10.21203/rs.3.rs-586610/v1

Stiubianu, G., Racles, C., Nistor, A., Cazacu, M., & Simionescu, B. C. (2011). Cellulose modification by crosslinking with siloxane diacids. *Cellulose Chemistry and Technology, 45*(3–4), 157–162.

Sun, X., Lu, C., Zhang, W., Tian, D., & Zhang, X. (2013). Acetone-soluble cellulose acetate extracted from waste blended fabrics via ionic liquid catalyzed acetylation. *Carbohydrate Polymers, 98*(1), 405–411. https://doi.org/10.1016/j.carbpol.2013.05.089

van den Berg, C. (1984). Description of water activity of foods for engineering purposes by means of the GAB model of sorption. In B. M. McKenna (Ed.), *Engineering and Foods* (pp. 311–321). New York: Elsevier Applied Science.

Vopička, O., & Friess, K. (2014). Analysis of gas sorption in glassy polymers with the GAB model: An alternative to the dual mode sorption model. *Journal of Polymer Science, Part B: Polymer Physics, 52*(22), 1490–1495. https://doi.org/10.1002/polb.23588